NIH-PA Author Manuscript NIH-PA Author Manuscript NIH-PA Author Manuscript

32. Karkkainen MJ, et al. A model for gene therapy of human hereditary lymphedema. Proc Natl Acad Sci USA. 2001; 98:12677–12682. [PubMed: 11592985]
33. Galvagni F, et al. Endothelial cell adhesion to the extracellular matrix induces c-Src-dependent VEGFR-3 phosphorylation without the activation of the receptor intrinsic kinase activity. Circ Res. 2010; 106:1839–1848. [PubMed: 20431062]
34. Jakobsson L, et al. Endothelial cells dynamically compete for the tip cell position during angiogenic sprouting. Nat Cell Biol. 2010; 12:943–953. [PubMed: 20871601]
35. Wiktor-Jedrzejczak WW, Ahmed A, Szczylik C, Skelly RR. Hematological characterization of congenital osteopetrosis in op/op mouse. Possible mechanism for abnormal macrophage differentiation. J Exp Med. 1982; 156:1516–1527. [PubMed: 7130905]
36. Takeshita K, et al. Critical role of endothelial Notch1 signaling in postnatal angiogenesis. Circ Res. 2007; 100:70–78. [PubMed: 17158336]
37. Yamamizu K, et al. Convergence of Notch and β-catenin signaling induces arterial fate in vascular progenitors. J Cell Biol. 2010; 189:325–338. [PubMed: 20404113]
38. Hayashi H, Kume T. Foxc transcription factors directly regulate Dll4 and Hey2 expression by interacting with the VEGF-Notch signaling pathways in endothelial cells. PLoS One. 2008; 3:e2401. [PubMed: 18545664]
39. Burgering BM. A brief introduction to FOXOlogy. Oncogene. 2008; 27:2258–2262. [PubMed: 18391968]
40. Petrova TV, et al. Defective valves and abnormal mural cell recruitment underlie lymphatic vascular failure in lymphedema distichiasis. Nat Med. 2004; 10:974–981. [PubMed: 15322537]
41. Norrmen C, et al. FOXC2 controls formation and maturation of lymphatic collecting vessels through cooperation with NFATc1. J Cell Biol. 2009; 185:439–457. [PubMed: 19398761]
42. Laakkonen P, et al. Vascular endothelial growth factor receptor 3 is involved in tumor angiogenesis and growth. Cancer Res. 2007; 67:593–599. [PubMed: 17234768]
43. Davis GE, Senger DR. Endothelial extracellular matrix: biosynthesis, remodeling, and functions during vascular morphogenesis and neovessel stabilization. Circ Res. 2005; 97:1093–1107. [PubMed: 16306453]
44. Zhang L, et al. VEGFR-3 ligand-binding and kinase activity are required for lymphangiogenesis but not for angiogenesis. Cell Res. 2010; 20:1319–1331. [PubMed: 20697430]
45. Nilsson I, et al. VEGF receptor 2/-3 heterodimers detected *in situ* by proximity ligation on angiogenic sprouts. EMBO J. 2010; 29:1377–1388. [PubMed: 20224550]
46. Wang Y, et al. Ephrin-B2 controls VEGF-induced angiogenesis and lymphangiogenesis. Nature. 2010; 465:483–486. [PubMed: 20445537]
47. Sawamiphak S, et al. Ephrin-B2 regulates VEGFR2 function in developmental and tumour angiogenesis. Nature. 2010; 465:487–491. [PubMed: 20445540]
48. Saharinen P, et al. Claudin-like protein 24 interacts with the VEGFR-2 and VEGFR-3 pathways and regulates lymphatic vessel development. Genes Dev. 2010; 24:875–880. [PubMed: 20439428]
49. Whitaker GB, Limberg BJ, Rosenbaum JS. Vascular endothelial growth factor receptor-2 and neuropilin-1 form a receptor complex that is responsible for the differential signaling potency of VEGF(165) and VEGF(121). J Biol Chem. 2001; 276:25520–25531. [PubMed: 11333271]
50. Carmeliet P, et al. Targeted deficiency or cytosolic truncation of the VE-cadherin gene in mice impairs VEGF-mediated endothelial survival and angiogenesis. Cell. 1999; 98:147–157. [PubMed: 10428027]
51. Shawber CJ, et al. Notch alters VEGF responsiveness in human and murine endothelial cells by direct regulation of VEGFR-3 expression. J Clin Invest. 2007; 117:3369–3382. [PubMed: 17948123]
52. Ober EA, et al. Vegfc is required for vascular development and endoderm morphogenesis in zebrafish. EMBO Rep. 2004; 5:78–84. [PubMed: 14710191]
53. De Palma M, Venneri MA, Roca C, Naldini L. Targeting exogenous genes to tumor angiogenesis by transplantation of genetically modified hematopoietic stem cells. Nat Med. 2003; 9:789–795. [PubMed: 12740570]

NIH-PA Author Manuscript NIH-PA Author Manuscript NIH-PA Author Manuscript

54. Mäkinen T, et al. Isolated lymphatic endothelial cells transduce growth, survival and migratory signals via the VEGF-C receptor VEGFR-3. EMBO J. 2001; 20:4762–4773. [PubMed: 11532940]
55. Soriano P. Generalized lacZ expression with the ROSA26 Cre reporter strain. Nat Genet. 1999; 21:70–71. [PubMed: 9916792]
56. Iida K, et al. Essential roles of the winged helix transcription factor MFH-1 in aortic arch patterning and skeletogenesis. Development. 1997; 124:4627–4638. [PubMed: 9409679]
57. Pytowski B, et al. Complete and specific inhibition of adult lymphatic regeneration by a novel VEGFR-3 neutralizing antibody. J Natl Cancer Inst. 2005; 97:14–21. [PubMed: 15632376]
58. Prewett M, et al. Antivascular endothelial growth factor receptor (fetal liver kinase 1) monoclonal antibody inhibits tumor angiogenesis and growth of several mouse and human tumors. Cancer Res. 1999; 59:5209–5218. [PubMed: 10537299]
59. Weijzen S, et al. The Notch ligand Jagged-1 is able to induce maturation of monocyte-derived human dendritic cells. J Immunol. 2002; 169:4273–4278. [PubMed: 12370358]
60. Tammela T, et al. Angiopoietin-1 promotes lymphatic sprouting and hyperplasia. Blood. 2005; 105:4642–4648. [PubMed: 15746084]
61. Baluk P, et al. Pathogenesis of persistent lymphatic vessel hyperplasia in chronic airway inflammation. J Clin Invest. 2005; 115:247–257. [PubMed: 15668734]
62. Ruhrberg C, et al. Spatially restricted patterning cues provided by heparin-binding VEGF-A control blood vessel branching morphogenesis. Genes Dev. 2002; 16:2684–2698. [PubMed: 12381667]
63. Karpanen T, et al. Lymphangiogenic growth factor responsiveness is modulated by postnatal lymphatic vessel maturation. Am J Pathol. 2006; 169:708–718. [PubMed: 16877368]
64. Zheng W, et al. Notch restricts lymphatic vessel sprouting induced by vascular endothelial growth factor. Blood. 2011; 118:1154–1162. [PubMed: 21566091]
65. Tvorogov D, et al. Effective suppression of vascular network formation by combination of antibodies blocking VEGFR ligand binding and receptor dimerization. Cancer Cell. 2010; 18:630–640. [PubMed: 21130043]
66. Jussila L, et al. Lymphatic endothelium and Kaposi's sarcoma spindle cells detected by antibodies against the vascular endothelial growth factor receptor-3. Cancer Res. 1998; 58:1599–1604. [PubMed: 9563467]
67. Ghalamkarpour A, et al. Recessive primary congenital lymphoedema caused by a VEGFR3 mutation. J Med Genet. 2009; 46:399–404. [PubMed: 19289394]
68. Persaud K, et al. Involvement of the VEGF receptor 3 in tubular morphogenesis demonstrated with a human anti-human VEGFR-3 monoclonal antibody that antagonizes receptor activation by VEGF-C. J Cell Sci. 2004; 117:2745–2756. [PubMed: 15150322]
69. Karpanen T, et al. Functional interaction of VEGF-C and VEGF-D with neuropilin receptors. FASEB J. 2006; 20:1462–1472. [PubMed: 16816121]
70. Jakobsson L, et al. Heparan sulfate in trans potentiates VEGFR-mediated angiogenesis. Dev Cell. 2006; 10:625–634. [PubMed: 16678777]
71. Lobov IB, et al. Delta-like ligand 4 (Dll4) is induced by VEGF as a negative regulator of angiogenic sprouting. Proc Natl Acad Sci USA. 2007; 104:3219–3224. [PubMed: 17296940]

METHODS

Mice and tissues

The study was approved by the Committee for Animal Experiments of the District of Southern Finland. The mice were anaesthetized with intraperitoneal injections of xylazine (10 mg kg^{-1}) and ketamine (80 mg kg^{-1}). The *Vegfr3*$^{+/LacZ}$ (ref. 8), *Vegfr3*$^{flox/flox}$ (ref. 17), *Vegfc*$^{+/LacZ}$ (ref. 15), *Vegfd*$^{+/-}$ (ref. 16), ROSA26-R (ref. 55), *Foxc2*$^{+/-}$ (ref. 56), *Csf1*$^{op/op}$ (ref. 35) and *Pdgfb–iCreER*^{T2} (ref. 29) mouse lines have been published previously. After killing the mice, tissues were immersed in 4% paraformaldehyde, washed in phosphate buffered saline (PBS) and then processed for whole-mount staining, immersed in OCT

NIH-PA Author Manuscript
NIH-PA Author Manuscript
NIH-PA Author Manuscript

medium (Tissue Tek) or embedded in paraffin. Deletion of *Vegfr3* in the *Pdgfb–iCreER^{T2};Vegfr3$^{flox/flox}$* mice was validated by immunohistochemistry and qRT-PCR (Supplementary Fig. S1). The possibility of a 3′ *Vegfr3* mRNA fragment originating from a cryptic start codon was excluded by qRT-PCR probes targeting the 5′ and 3′ ends of the *Vegfr3* transcript; no difference in expression levels was found (data not shown).

Analysis of angiogenesis in the postnatal mouse retina and in the embryonic mouse hindbrain

Neonatal *Pdgfb–iCreER^{T2}*; *Vegfr3$^{flox/flox}$*, *Pdgfb–iCreER^{T2};ROSA26-R* or control mice were intragastrically injected with 2 μl of 4-OHT (Sigma) dissolved in 97% ethanol, on P3 and P4 using a 10 μl Hamilton syringe. A 12 h induction of Cre activity with 4-OHT during P5 was sufficient to result in Cre-activated β-galactosidase reporter expression in most endothelial cells of the developing retinal vasculature; the strongest signal was observed in the tip cells (Supplementary Fig. S1a), which express high levels of *Pdgfb* (ref. 18). Induction for 48 h resulted in robust Cre-dependent β-galactosidase activity in all endothelial cells (Supplementary Fig. S1b). For the antibody treatments, NMRI pups were subcutaneously injected with 50 mg kg^{-1} of anti-VEGFR-3 (mF4-31C1; ref. 57) or anti-VEGFR-2 (DC101; ref. 58) on P3 and P4. The small peptide mimetic of the Notch ligand Jagged1 (Jag1) or scrambled control peptide (SC-Jag1, Thermo Scientific) was dissolved in 50% dimethylsulphoxide and 50% sterile water, and administered subcutaneously at 10 mg kg^{-1} (refs 19,59) on P3 and P4 at 12 h intervals. To identify proliferating endothelial cells, the pups were given 0.2 mg of 5-bromo-2-deoxyuridine (BrdU) by intraperitoneal injections, 2 h before being killed. In all cases, the pups were killed on P5, and their eyes were collected for analysis. For hindbrain analysis, pregnant females were given 2.5 mg of 4-OHT dissolved in 40% ethanol and 60% sunflower seed oil (Sigma), using a feeding needle at E10.5 (for 24 h analysis) or E10.5 and E11.5 (for 48 h analysis). Embryos were collected on E11.5 or E12.5, and hindbrains were processed for whole-mount immunohistochemistry.

Transduction of the mouse ear skin with adenoviral gene transfer vectors

Cre was induced at least 2 days in advance by subcutaneous implantation of sustained release pellets (21 days) containing tamoxifen (25 mg, Innovative Research). Adenoviruses encoding human VEGF$_{165}$ or VEGF-B$_{167}$ were injected intradermally into the ears of *Pdgfb–iCreER^{T2};Vegfr3$^{flox/flox}$* mice. A total of 2×10^8 plaque-forming units of each virus were injected in a volume of 50 μl. The mice were perfusion-fixed 5 days after injection, and the ears were collected and processed for whole-mount analysis[60], or immersed in OCT medium (Tissue Tek).

Tumour cell lines, xenografts and treatments

B16–F10–Luc2–G5 mouse melanoma or mouse LLC cells were maintained in DMEM, supplemented with 2 mM L-glutamine, penicillin (100 U ml^{-1}), streptomycin (100 μg ml^{-1}) and 10% fetal calf serum (Promo Cell). For B16–F10–Luc2–G5 cells, zeocin was added at a final concentration of 0.3 mg ml^{-1} as a selection marker. The B16 and LLC syngeneic grafts were made by injecting 2–4 × 10^6 cells into the subcutaneous space in the abdominal flank of *Pdgfb–iCreER^{T2};Vegfr3$^{flox/flox}$* mice. Again, Cre was induced by subcutaneous implantation of the sustained tamoxifen-release pellets (25 mg, Innovative Research).

Immunohistochemistry

50 μm sections of tumours and 10 μm sections of ears were fixed with cold acetone, washed with PBS and blocked with TNB (PerkinElmer). The following primary antibodies were

NIH-PA Author Manuscript NIH-PA Author Manuscript NIH-PA Author Manuscript

used for immunostaining of mouse tissues: polyclonal goat anti-mouse VEGFR-3 (R&D Systems, 1:50–1:100), rabbit polyclonal anti-GFP (TP401, Torrey Pines Biolabs, 1:1,000), unconjugated or fluorescein isothiocyanate (FITC)-conjugated rat anti-PECAM-1 (clone MEC 13.3, 553370, BD Pharmingen, 1:500, 1:800), rat anti-mouse endomucin (V.7C7: sc-65495, Santa Cruz Biotechnology, 1:100), polyclonal rabbit anti-FITC (Zymed/ Invitrogen, 1:100), rabbit anti-mouse collagen IV (LB-1403, Cosmo Bio, 1:1,000), rabbit #6 polyclonal antiserum to VEGF-C (ref. 61), or pre-immune rabbit #6 serum as a negative control[61], and Alexa-Fluor-594-conjugated mouse anti-BrdU monoclonal antibody (clone MoBU-1, B35132, Invitrogen, 1:500). Sections were washed with TNT buffer and the primary antibodies were detected with the appropriate Alexa 488, 594 or 647 secondary antibody conjugates (Molecular Probes/Invitrogen).

Hindbrains of E11.5 or E12.5 embryos were processed for whole-mount immunofluoresence staining as previously described[62]. For analysis of the microvasculature, retinas were stained with biotinylated *Griffonia simplicifolia* lectin (Vector Laboratories), as before[18], followed by immunostaining. Alternatively, to detect β-galactosidase activity, eyes were processed, as before[14]. After staining, retinas were washed and mounted in Vectashield (Vector Laboratories) or re-fixed in 4% paraformaldehyde and processed for whole-mount immunofluoresence staining. All fluorescently labelled samples were mounted with Vectashield containing 4,6-diamidino-2-phenylindole (DAPI, Vector Laboratories).

Microscopy

Fluorescently labelled samples were analysed with a compound fluorescent microscope (Zeiss 2, Carl Zeiss; ×10 objective with numerical aperture (NA) 0.30) or a confocal microscope (Zeiss LSM 510Meta, objectives ×10 with NA 0.45, oil objectives ×40 with NA 1.3 and ×63 with NA 1.4; or Zeiss LSM 5 Duo, objectives ×10 with NA 0.45, oil objectives ×40 with NA 1.3 and ×63 with NA 1.4) using multichannel scanning in frame mode, as before[14]. Three-dimensional projections were digitally reconstructed from confocal *z* stacks. Co-localization of signals was assessed from single confocal optical sections. Images of whole retinas were acquired using tile scanning with a pinhole diameter >3.0 Airy units. X-gal (5-bromo-4-chloro-3-indolyl-β-D-galactoside) staining of LacZ reporter mice was analysed with a Leica DM LB camera (objectives ×10 with NA 0.25 and ×20 with NA 0.4).

Cell culture and reagents

hBECs (PromoCell) were maintained in endothelial cell growth medium (ECGM, PromoCell, C22120) with supplements provided by the manufacturer. For stimulation experiments, hBECs were starved for 6–8 h in serum-free ECGM and stimulated for 1 or 2 h in fresh starvation media. The following reagents were used: human VEGF (100 ng ml^{-1}, 293-VE, R&D) and VEGF-$C^{\Delta N\Delta C}$ (200 ng ml^{-1}; ref. 63). For Notch or PI(3)K inhibition experiments, cells were starved for 6 h and Dll4-Fc (Dll4-Fc conditioned medium[64]), LY294002 (10 μM, 440204, Calbiochem) or PD98059 (20 μM, Calbiochem) was added for 30, 15 and 30 min respectively before stimulation with VEGF-C (200 ng ml^{-1}, added in the same media). For silencing experiments, hBECs were transfected with human *VEGFR3* or non-targeted siRNA (Thermo Scientific Dharmacon siGENOME ON-TARGETplus SMARTpool reagents), using Oligofectamine (Invitrogen). For activation of Notch in cultured hBECs, 50% of the cells were transduced with pMX retroviral vectors expressing mouse Dll4–ECTM–eGFP (mDll4–ECTM–eGFP; ref. 64). Gene expression was examined 48 h post-transfection by qRT-PCR from cells lysed in RLT buffer (Qiagen). Alternatively, cells were lysed in PLCLB lysis buffer (150 mM NaCl, 5% glycerol, 1% Triton X-100, 1.5 M $MgCl_2$, 50 mM HEPES, pH 7.5, 1 mM Na_3VO_4, phenylmethylsulphonyl fluoride, leupeptin and aprotinin) for western blotting[65], using the following antibodies: goat anti-

NIH-PA Author Manuscript NIH-PA Author Manuscript NIH-PA Author Manuscript

mouse VEGFR-2 (AF357, R&D Systems), goat anti-mouse VEGFR-3 (AF743, R&D Systems), mouse anti-human VEGFR-3 (clone 9D9, ref. 66), rabbit anti-human β-actin (#4967, Cell Signaling) and mouse anti-phosphotyrosine (#05-321, Millipore).

Analysis of VEGFR-3 phosphorylation following adhesion to collagen I

hBECs were transfected with pMX retrovirus encoding VEGFR3–StreptagII (ref. 67), detached using Accutase (PAA Laboratories) and plated on Collagen I or poly-L-lysine (both 4 μg cm^{-2}), which was used as a control. Cells were then incubated for the indicated times depending on the experimental set-up with 1 μg ml^{-1} 3C5 (ref. 68), 1 nM cediranib (Astra Zeneca) or 1 mM PP2 (Calbiochem). VEGFR-3 was precipitated from PLCLB lysates using Strep-Tactin beads (IBA). After that proteins were analysed by western blotting using antibodies to pTyr or VEGFR-3.

Analysis of VEGFR-3 and VEGFR-2 phosphorylation in *ex vivo* embryo cultures

E10.5–E11.5 NMRI wild-type embryos were excised from amnionic sacs and placed in Dulbecco's modified Eagle's medium (DMEM) containing 0.2% bovine serum albumin (BSA) on ice. The embryos were injected through the outflow tract with 0.5 ml of DMEM containing 100 ng ml^{-1} recombinant human $VEGF_{165}$ (R&D Systems), 200 ng ml^{-1} VEGF-$C^{\Delta N\Delta C}$ (ref. 69) or 0.2% BSA. Altogether 10–15 embryos were used in each group. Embryos were placed in DMEM containing the same concentration of growth factors, incubated at 37 °C for 20 min and lysed in 1% Triton X-100, 40 mM Tris-HCl (pH 7.5), 150 mM NaCl, 2 mM Na_3VO_4, 100 μM phenylmethylsulphonyl fluoride, 50 mM NaF and 10 μg ml^{-1} of both aprotinin and leupeptin. Insoluble materials were removed by centrifugation at 14,000*g* for 15 min.

PI(3)K activity assay

hBECs were incubated on 96-well plates (10^4 cells per well) and silenced with human *VEGFR3* or non-targeting siRNA for 48 h, before stimulating with VEGF (100 ng ml^{-1}) or VEGF-C (200 ng ml^{-1}) for 15 min. PI(3)K activity was evaluated using FACE PI3-kinase p85 ELISA Kit (Active Motif) according to the manufacturer's instructions. The signal was normalized to cell numbers by staining with crystal violet. PI(3)K activity was measured with a microplate reader (Thermo Labsystems Multiscan Ascent).

Three-dimensional cultures of embryoid bodies

Embryonic stem cells were routinely cultured on a layer of irradiated DR4 mouse embryonic fibroblasts in the presence of leukaemia inhibitory factor (LIF). For vascular sprouting experiments, cells were cultured for two passages without feeders, trypsinized, depleted of LIF, followed by mixing of wild-type (DsRed) and $Vegfr3^{+/LacZ}$ cells in a 1:1 ratio and left in suspension (day 0). On day 4, embryoid bodies were embedded in a polymerized collagen I gel (as previously described[70]) with the addition of 30 ng ml^{-1} $mVEGF_{164}$ (Peprotech) with dimethylsulphoxide or DAPT (5 μM, Sigma-Aldrich). Medium was changed on day 6 and every day thereafter.

qRT-PCR

Total RNA from retinas, collected at P5, or hBECs was isolated using the RNeasy Mini Kit (Qiagen) or the NucleoSpin RNA II Kit (Macherey-Nagel). Homogenization was carried out using rotor-stator homogenization, followed by on-column DNase digestion (RNase-Free

NIH-PA Author Manuscript NIH-PA Author Manuscript NIH-PA Author Manuscript

DNase Set, 79254). Quality control of samples was carried out using a Nanodrop ND-1000 spectrophotometer. RNA was reverse-transcribed using the DyNAmo cDNA Synthesis Kit (F-470L, Finnzymes) or the iScript cDNA Synthesis Kit (Bio-Rad) according to the manufacturer's instructions. Three qRT-PCR reactions were carried out from every *in vitro* transcription reaction using TaqMan Gene Expression Assays (Applied Biosystems) and the DyNAmo Probe qPCR Kit (F-450S, Finnzymes) or the iQ Supermix Kit (Bio-Rad). qRT-PCR was carried out using a BIO-RAD C1000 Thermal cycler according to a standardized protocol. The TaqMan Gene Expression Assays used for mouse mRNA were: *Gapdh* (4352932E), *Cadh5* (Mm00486938_m1), *Pdgfb* (Mm00440678_m1), *Vegfr1* (Mm00438980_m1), *5'-Vegfr3* (Mm01292608_m1), *3'-Vegfr3* (Mm00433354_m1), *Nrarp* (Mm00482529_s1), *Hey1* (Mm00468865_m1), *Hey2* (Mm00469280_m1), *Dll4* (Mm00444619_m1), *Notch1* (Mm00435245_m1), *Notch4* (Mm00440525_m1) and *Foxc2* (Mm01250130_s1). At least three retinas from *Pdgfb–iCreER^{T2}*; *Vegfr3$^{flox/flox}$* and *Vegfr3$^{flox/flox}$* littermates were used for analysis at P5.

The TaqMan Gene Expression Assays used for human RNA were: *GAPDH* (Hs99999905_m1), *HEY1* (Hs01114113_m1), *HEY2* (Hs00232622_m1), *NRARP* (Hs01104102_s1), *DLL4* (Hs01117332_g1), *NOTCH1* (Hs01062014_m1), *NOTCH4* (Hs00965895_g1) and *FOXC2* (Hs00270951_s1). The data were normalized to the endogenous controls *Gapdh* or *Cadh5* and *GAPDH* in murine and human samples, respectively. At least three independent experiments per condition were analysed. Fold changes were calculated using the comparative CT (threshold cycle) method.

Vessel morphometry and quantitative analysis

The vascular surface area in retinas was quantified as an isolectin-B4-positive area from ×10 confocal micrographs acquired of all intact quarters of the processed retina and at a similar distance from the optic nerve using Image J software, as described previously[14]. PECAM-1-positive vessels from thick tumour sections were quantified from 1.69 mm^2 micrographs from regions of uniform staining intensity in a similar manner. PECAM-1-positive vessels in the ear sections were quantified from images that were acquired using tile-scanning mode with a pinhole diameter >3 Airy units. Vessel branching points, sprouts and filopodia number were counted manually from fluorescence micrographs of retinas, as described previously[71]. For each hindbrain, the number of sprouting vessels on the pial side and the number of branching points on the subventricular zone were determined in 3–6 randomly chosen 0.85 mm^2 fields. At least two litters of embryos per embryonic stage were independently analysed. Images were edited using PhotoShop software (Adobe).

Statistical analysis

Statistical analysis was carried out using PASW Statistics 18.0. A two-tailed Student *t*-test, paired Student *t*-test or one-way analysis of variance (ANOVA) was used for statistical analysis. A *P* value of less than 0.05 was considered to be statistically significant.

NIH-PA Author Manuscript NIH-PA Author Manuscript NIH-PA Author Manuscript

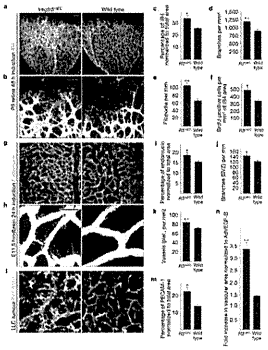

Figure 1.

Blood vascular hyperplasia and excessive filopodia projection in mice with a targeted deletion of *Vegfr3* in the endothelium. (**a,b**) Visualization of blood vessels by isolectin B4 (iB4) staining of *Vegfr3*$^{i\Delta EC}$ and wild-type littermate retinas at P5. Yellow dots indicate filopodia at the vascular front in **b**. Scale bars, 100 μm (**a**) and 50 μm (**b**). (**c–f**) Quantitative analysis of the retinas shown in **a** and **b**. (**c**) iB4-positive surface area normalized to total area. (**d**) Number of vessel branching points. (**e**) Number of filopodia per length of vascular front. (**f**) BrdU-positive cells per iB4 area (see Supplementary Fig. S2). In all cases, Cre activity was induced for 48 h before the mice were killed. **c–e** show data from one litter containing 5 *Vegfr3*$^{i\Delta EC}$ and 3 wild-type mice. (**f**) Data from one litter containing 3 *Vegfr3*$^{i\Delta EC}$ and 4 wild-type mice. (**g,h**) Endomucin staining of E11.5 mouse hindbrains after Cre induction for 24 h before the mice were killed. Yellow asterisks indicate the hindbrain midline in **g**, and yellow dots indicate filopodia in **h**. Scale bars, 100 μm (**g**) and 20 μm (**h**). (**i–k**) Quantitative analysis of the *Vegfr3*$^{i\Delta EC}$ and wild-type hindbrains; n =3 *Vegfr3*$^{i\Delta EC}$ and 5 wild-type embryos. (**i**) Endomucin-positive surface area normalized to total area. (**j**) Number of vessel branching points in the subventricular side. (**k**) Number of vessel sprouts in the pial side (see Supplementary Fig. S3). (**l**) PECAM-1 staining of LLC tumour xenografts 11 days after implantation into *Vegfr3*$^{i\Delta EC}$ or wild-type littermate mice. Scale bar, 50 μm. (**m**) Quantification of PECAM-1-positive area in the tumours shown in **l**; n = 5 *Vegfr3*$^{i\Delta EC}$ and 5 wild-type mice. (**n**) Fold increase in vascular area 4 days after transduction with adenoviral vectors encoding VEGF (AdVEGF), normalized to AdVEGF-B in *Vegfr3*$^{i\Delta EC}$ versus wild-type mice (see Supplementary Fig. S4); n =3 ears per group. $^{**}P$ <0.005, $^{*}P$ <0.05. Error bars, s.e.m.

NIH-PA Author Manuscript

NIH-PA Author Manuscript

NIH-PA Author Manuscript

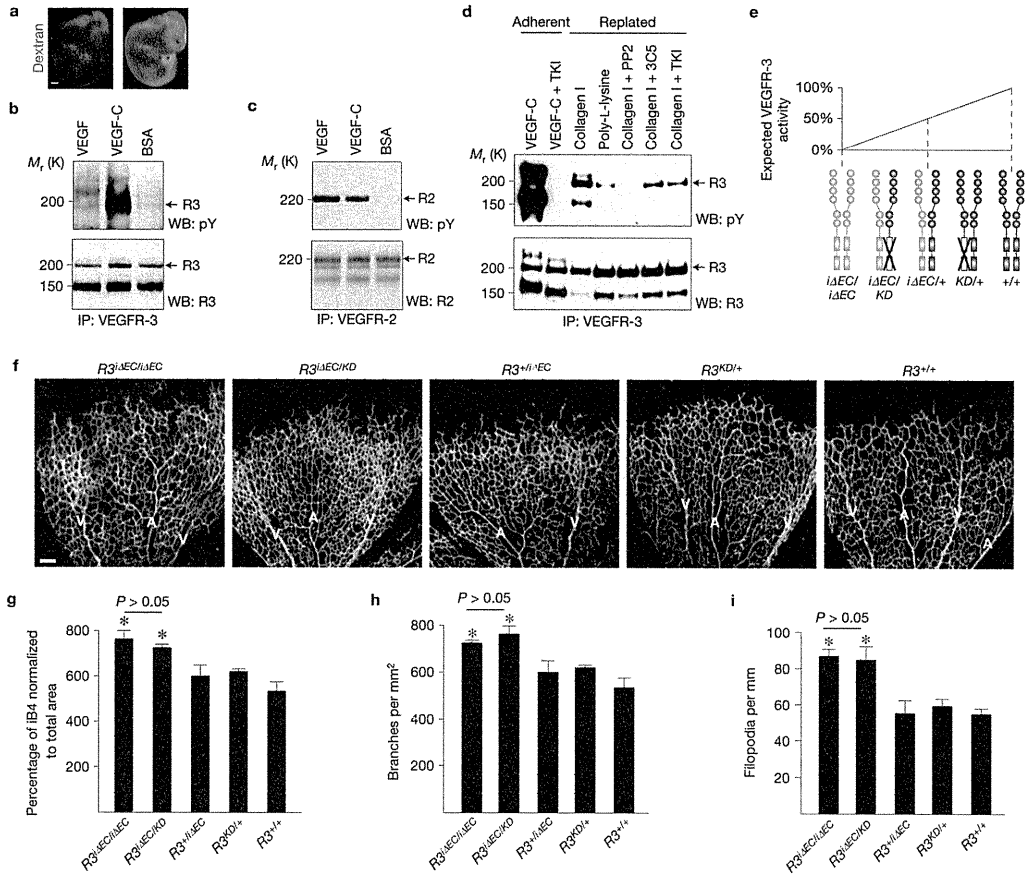

Figure 2.

Role of VEGFR-3 tyrosine kinase activity in angiogenesis. (**a**) Intra-embryonic injection of FITC–dextran (green) into the cardiac outflow tract at E11.5 showing homogeneous perfusion of the embryo. Scale bar, 200 μm. (**b,c**) Immunoprecipitation (IP) of VEGFR-3 (**b**) or VEGFR-2 (**c**) of embryos stimulated with VEGF, VEGF-C or BSA followed by western blotting (WB) for phosphotyrosine (pY), VEGFR-3 (R3) or VEGFR-2 (R2). $N = 9$ (**b**) and 8 (**c**) embryos per lane. (**d**) Immunoprecipitation of VEGFR-2 from hBECs transduced with pMX–VEGFR3–StreptagII retrovirus. Adherent cells were stimulated with VEGF-C, whereas detached cells were replated on collagen I or poly-L-lysine, and subjected to the indicated inhibitors. Uncropped images of blots are shown in Supplementary Fig. S9a. (**e**) Schematic illustration showing the expected VEGFR-3 activity following the indicated genetic perturbations of *Vegfr3*. (**f**) iB4 staining of mouse retinas at P5 48 h after 4-OHT administration. A, artery; V, vein. Scale bar, 100 μm. (**g–i**) Quantitative analysis of the retinas shown in **f**. (**g**) Isolectin B4 (iB4)-positive surface area normalized to total area. (**h**) Number of vessel branching points. (**i**) Number of filopodia per length of vascular front. Data pooled from 4 litters containing altogether 8 *iΔEC/iΔEC*, 4 *iΔEC/KD*, 6 *+/iΔEC*, 5 *KD/+* and 7 wild-type pups. $^{*}P<0.05$. Error bars, s.e.m.

NIH-PA Author Manuscript NIH-PA Author Manuscript NIH-PA Author Manuscript

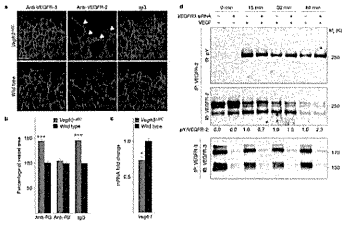

Figure 3.

An increased level of VEGFR-2 signalling contributes to vascular hyperplasia in *Vegfr3*$^{i\Delta EC}$ retinas. (**a**) Isolectin B4 staining (in green) of *Vegfr3*$^{i\Delta EC}$ retinas after treatment with VEGFR-3- or VEGFR-2-blocking antibodies during P3–P5. Non-specific rat IgG was used as a control. Arrowheads indicate abnormally thick vessels. Scale bar, 100 μm. (**b**) Statistical analysis showing the percentage vessel area increase in *Vegfr3*$^{i\Delta EC}$ versus wild-type littermate mice in every treatment group (individual experiments; $n = 4$, 5 and 4 *Vegfr3*$^{i\Delta EC}$ pups treated with anti-VEGFR-3, anti-VEGFR-2 and IgG, respectively; and 6, 3 and 5 wild-type pups treated with anti-VEGFR-3, anti-VEGFR-2 and IgG, respectively). (**c**) qRT-PCR analysis of *Vegfr1* gene (also known as *Flt1*) expression; $n = 4$ *Vegfr3*$^{i\Delta EC}$ and 3 wild-type pups. In all analyses of the retina, Cre activity was induced for 48h before the mice were killed. $^{*}P < 0.05$, $^{***}P < 0.001$. Error bars, s.e.m. (**d**) Cultured HUVECs subjected to siRNA-mediated silencing of *VEGFR3* expression (*VEGFR3* siRNA) and stimulation with VEGF for the indicated times. VEGFR-2 was immunoprecipitated (IP) followed by immunoblotting (IB) for phosphotyrosine (pY) and VEGFR-2. Numbers below the blots indicate relative intensities of pY to VEGFR-2, normalized to control siRNA at the same time point. Note the increased pVEGFR-2 signal at 30 min and 60min (red). Immunoprecipitation and western blot analysis for VEGFR-3 from the same lysates is shown below. Uncropped images of blots are shown in Supplementary Fig. S9b.

NIH-PA Author Manuscript
NIH-PA Author Manuscript
NIH-PA Author Manuscript

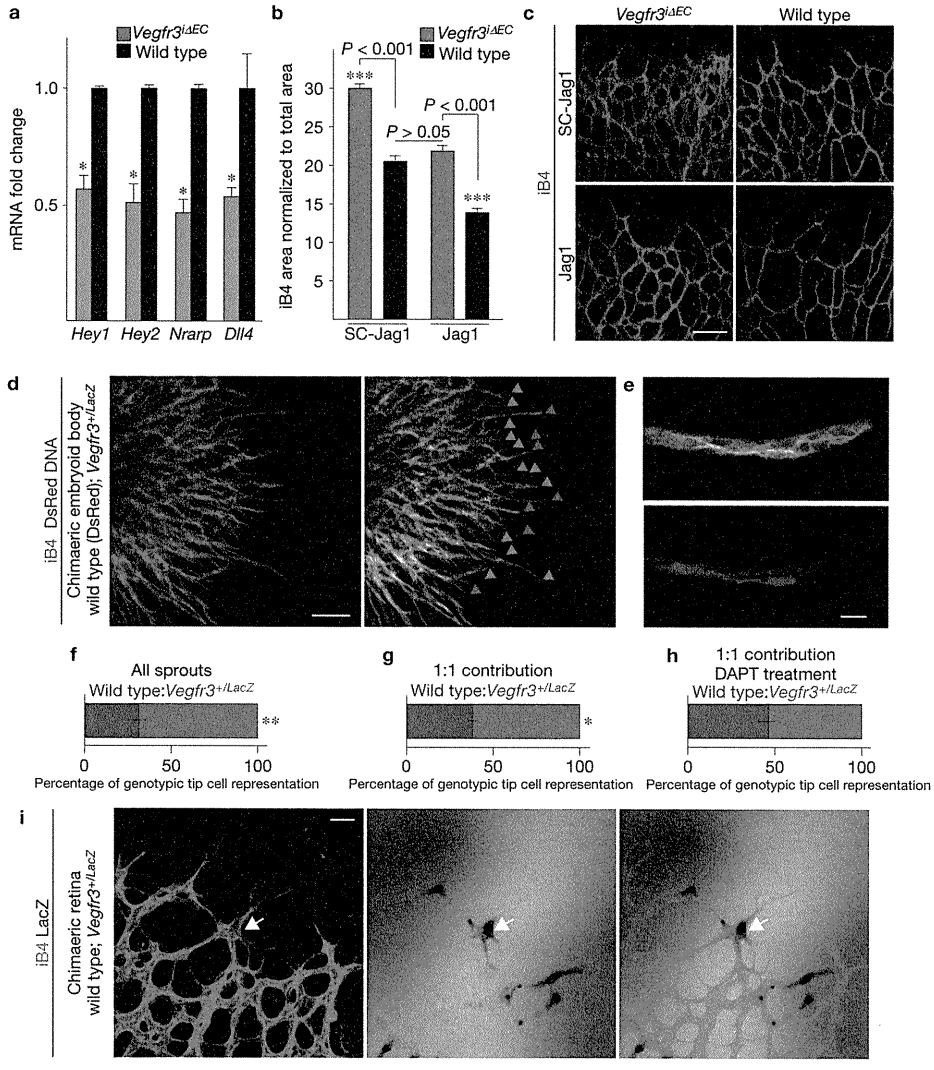

Figure 4.

A decreased level of Notch signalling underlies excessive angiogenesis in *Vegfr3*$^{i\Delta EC}$ retinas. (**a**) Fold changes in *Hey1, Hey2, Nrarp* and *Dll4* mRNA levels in the retinas of *Vegfr3*$^{i\Delta EC}$ and wild-type littermate pups at P5. mRNA levels were normalized to *Cadh5* to compensate for the increased endothelial cell numbers in *Vegfr3*$^{i\Delta EC}$ retinas. $^{*}P < 0.05$; n = 4 *Vegfr3*$^{i\Delta EC}$ and 3 wild-type pups. Error bars, s.e.m. (**b,c**) Vessel area quantification (**b**) and isolectin B4 (iB4) staining (**c**) of *Vegfr3*$^{i\Delta EC}$ and wild-type littermate retinas at P5 following administration of Jagged1 peptide mimetics (Jag1) or scrambled peptides (SC-Jag1) and 4-OHT for 48h. Scale bar, 100 μm. $^{***}P < 0.001$; n = 3 *Vegfr3*$^{i\Delta EC}$ and 4 wild-type pups treated with SC-Jag1 and 4 *Vegfr3*$^{i\Delta EC}$ and 4 wild-type pups treated with Jag1. Data pooled from 2 individual experiments. Error bars, s.e.m. (**d**) A 10 day chimaeric embryoid body derived from wild-type DsRed-expressing embryonic stem cells (red), mixed in a 1:1 ratio with embryonic stem cells having one functional *Vegfr3* allele (*Vegfr3*$^{+/LacZ}$) and stained for iB4 (green). Red arrowheads indicate tip cells of wild-type origin; green arrowheads point to *Vegfr3* heterozygous cells. Scale bar, 200 μm. (**e**) High-magnification image of a sprout showing a mosaic distribution of the cells. DNA in blue. Scale bar, 20 μm. (**f,g**) Quantification of the tip cell genotype in all sprouts (**f**; 65.89%±2.5% s.e.m.; n = 621 sprouts), in sprouts that exhibited a 1:1 contribution of wild-type and *Vegfr3*$^{+/LacZ}$ cells (**g**;

NIH-PA Author Manuscript NIH-PA Author Manuscript NIH-PA Author Manuscript

61.8%± 1.8% s.e.m.; $n = 360$ sprouts) and in sprouts with a 1:1 contribution of wild-type and *Vegfr3*$^{+/LacZ}$ cells following treatment with DAPT (**h**; 53.7%±2.7% s.e.m.; $n = 325$ sprouts). $^{**}P < 0.01$, $^{**}P < 0.05$. Error bars, s.e.m. (**i**) Mosaic retina of a P5.5 pup derived from a wild-type blastocyst injected with *Vegfr3*$^{+/LacZ}$ embryonic stem cells and stained for iB4. β-galactosidase activity (in black, arrow) indicates a *Vegfr3*$^{+/LacZ}$ cell. Scale bar, 50 μm.

NIH-PA Author Manuscript
NIH-PA Author Manuscript
NIH-PA Author Manuscript

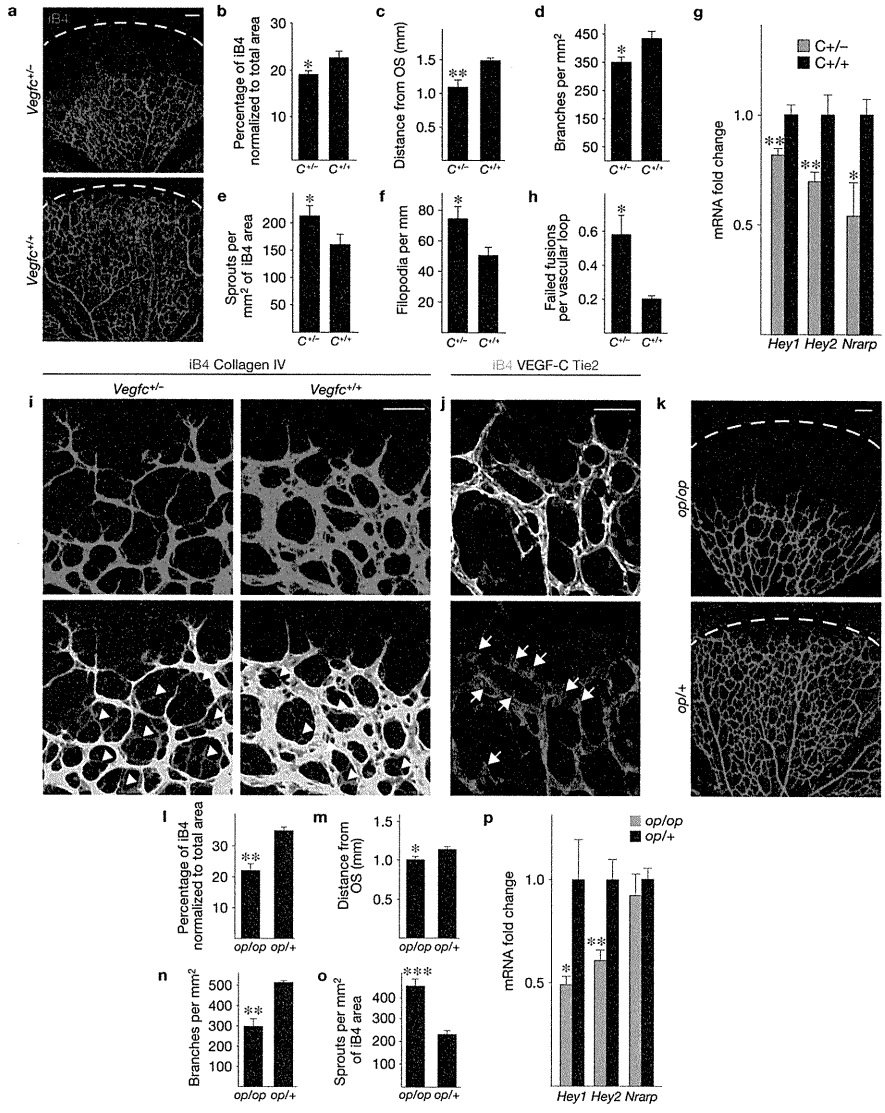

Figure 5.

Vegfc haploinsufficiency leads to instability of sprout fusion points and inefficient angiogenesis. (**a**) Isolectin B4 (iB4) staining (green) of retinas from *Vegfc*$^{+/-}$ mice and their wild-type littermates at P5. (**b–f**) Quantitative analysis of the retinas shown in **a**; data pooled from two litters containing altogether 6 *Vegfc*$^{+/-}$ and 9 wild-type pups. (**b**) iB4-positive surface area normalized to total area. (**c**) Extent of vascular plexus migration from the optic stalk (OS). (**d**) Number of vessel branching points. (**e**) Number of sprouts. (**f**) Filopodia per length of vascular front. (**g**) Fold changes in *Hey1*, *Hey2* and *Nrarp* mRNA levels analysed by qRT-PCR in the retinas of *Vegfc*$^{+/-}$ and wild-type pups at P5 (data pooled from two litters containing altogether 7 *Vegfc*$^{+/-}$ and 6 wild-type pups). (**h**) Number of failed fusions per vascular loop in the retinas of *Vegfc*$^{+/-}$ and *Vegfc*$^{+/+}$ pups at P5 ($n = 6$ *Vegfc*$^{+/-}$ and 9 wild-type pups, data pooled from 2 litters). (**i**) iB4 (green) and collagen IV (red) staining of *Vegfc*$^{+/-}$ or wild-type littermate retinas at P5. Arrowheads indicate empty basement membrane sleeves. (**j**) iB4 (white), VEGF-C (red) and Tie2 (green) immunostaining in wild-type mouse retinas at P5. Arrows indicate VEGF-C- and Tie2-positive macrophages at the angiogenic front. (**k**) iB4 staining (green) of P5 retinas of *op/op* pups and *op/+* littermate controls. (**l–o**) Quantitative analysis of the retinas shown in **k**; $n = 5$ *op/op* and 4 *op/+* pups.

NIH-PA Author Manuscript NIH-PA Author Manuscript NIH-PA Author Manuscript

Dashed line in **a** and **k** indicates a similar distance from the optic stalk (OS). (**l**) iB4-positive surface area normalized to total area. (**m**) Extent of vascular plexus migration from the optic stalk. (**n**) Number of vessel branching points. (**o**) Number of sprouts. (**p**) Fold changes in *Hey1, Hey2* and *Nrarp* mRNA levels analysed by qRT-PCR in the retinas of *op/op* pups and *op/+* pups at P5 *(n* = 5 *op/op* and 3 *op/+* pups). Scale bars, 100 μm (**a,k**) and 50 μm (**i,j**). * $P < 0.05$, ** $P < 0.01$, $^{***}P < 0.001$. Error bars, s.e.m.

NIH-PA Author Manuscript
NIH-PA Author Manuscript
NIH-PA Author Manuscript

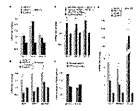

Figure 6.

VEGF-C promotes Notch signalling in endothelial cells through VEGFR-3 and PI(3)K. (**a**–**d**) Fold changes in Notch target gene and *DLL4* levels in hBECs stimulated with 200 ng ml^{-1} VEGF-C, and treated with Dll4-Fc conditioned medium (**a**), transfected with *VEGFR3* siRNA or control siRNA (**b**), in conditions where 50% of hBECs express membrane-bound Dll4 (Dll4-TM; **c**) or treated with the PI(3)K inhibitor LY294002 (**d**). Cells were stimulated for 1 h before lysis. Expression of *GAPDH* was used as the normalization control. Note the successful transduction of hBECs with retroviruses encoding Dll4-TM in **c**, as evaluated by qRT-PCR. (**e**) Fold increase in PI(3)K activity in *VEGFR3* versus control silenced hBECs after stimulation with VEGF-C (100 ng ml^{-1}) for 15 min. Data pooled from 2 individual experiments, each containing 3 replicates. * denotes *P* values versus control group ($^{*}P$ <0.05, $^{**}P$ <0.01, $^{***}P$ <0.001) and # denotes *P* values between groups (# *P* <0.05, ## *P* <0.01). Error bars, s.e.m.

NIH-PA Author Manuscript
NIH-PA Author Manuscript
NIH-PA Author Manuscript

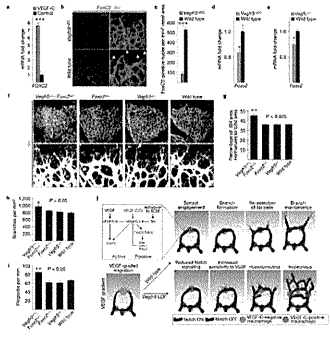

Figure 7.

VEGFR-3 interacts with the transcription factor FoxC2 to control angiogenesis. (**a**) Fold change in the level of *FOXC2* mRNA expression following stimulation of hBECs with 200 ng ml^{-1} VEGF-C ($n = 3$ plates per group). (**b**) Immunostaining for FoxC2 (red) and isolectin B4 (iB4; green) in $Vegfr3^{i\Delta EC}$ and wild-type littermate pups at P5. Arrowheads indicate FoxC2-negative tip cells. (**c**) Quantification of FoxC2-positive nuclei from the retinas shown in **b**. Nuclei in the area of iB4-positive endothelial cells were quantified at the angiogenic front ($n = 3$ pups per group). (**d,e**) Fold change in the level of *Foxc2* mRNA expression in $Vegfr3^{i\Delta EC}$ and wild-type littermate retinas (**d**), and in $Vegfc^{+/-}$ or wild-type littermate retinas (**e**) at P5 ($n = 3$ pups per group). (**f**) iB4 staining (white) in $Foxc2^{+/-}$; $Vegfr3^{+/-}$, $Foxc2^{+/-}$, $Vegfr3^{+/-}$ or wild-type littermate retinas at P5. Yellow dots in the lower panels indicate filopodia. (**g–i**) Quantitative analysis of the retinas shown in **f**. (**g**) iB4-positive surface area normalized to total area. (**h**) Number of vessel branching points. (**i**) Filopodia per length of vascular front. Data pooled from 2 litters; $n = 3$ $Foxc2^{+/-}$; $Vegfr3^{+/-}$, 4 $Foxc2^{+/-}$, 4 $Vegfr3^{+/-}$ and 4 wild-type pups. Scale bars, 50 μm. $^{*}P<0.05$, $^{**}P<0.01$, $^{***}P<0.001$. Error bars, s.e.m. (**j**) Schematic of VEGF-C-expressing macrophages in vessel anastomosis and branch maintenance during developmental angiogenesis. Initially, 2 tip cells that lead vascular sprouts are chaperoned to fuse by a macrophage (green). VEGF-C expression (purple) ensues in the macrophage, activating VEGFR-3 in the tip cells, which leads to the expression of Notch target genes and decreased sensitivity to the VEGF gradient in the cells. *Vegfr3* loss-of-function (LOF) leads to decreased Notch signalling. A simplified summary of the 'active' (green) and 'passive' (red) signalling pathways originating from VEGFR-3 is shown in the upper left corner. Only the 'active' pathway is targetable by inhibitors.

Gene 496 (2012) 79–87

Contents lists available at SciVerse ScienceDirect

Gene

journal homepage: www.elsevier.com/locate/gene

Detergent-induced activation of the hepatitis C virus genotype 1b RNA polymerase

Leiyun Weng [a], Michinori Kohara [b], Takaji Wakita [c], Kunitada Shimotohno [d], Tetsuya Toyoda [a,b,e,*]

[a] Unit of Viral Genome Regulation, Institut Pasteur of Shanghai, Key Laboratory of Molecular Virology & Immunology, Chinese Academy of Sciences, 411 Hefei Road, Shanghai 200025, PR China
[b] Infectious Disease Regulation Project, Tokyo Metropolitan Institute of Medical Sciences, 1-6, Kamikitazawa 2-chome, Setagaya-ku, Tokyo 156-8506, Japan
[c] Department of Virology II, National Institute of Health, 1-23-1 Toyama, Shinjuku, Tokyo 132-8640, Japan
[d] Affiliated Research Institute, Chiba Institute of Technology, 2-17-1 Tsudamuna, Narashino, Chiba 275-0016, Japan
[e] Choju Medical Institute, Fukushimura Hospital, 19-4 Azanakayama, Noyori-cho, Toyohashi, Aichi 441-8124, Japan

ARTICLE INFO

Article history:
Accepted 18 January 2012
Available online 28 January 2012

Keywords:
HCV
NS5B
RNA polymerase
In vitro transcription
Triton X-100
Oligomer

ABSTRACT

Recently, we found that sphingomyelin bound and activated hepatitis C virus (HCV) 1b RNA polymerase (RdRp), thereby recruiting the HCV replication complex into lipid raft structures. Detergents are commonly used for resolving lipids and purifying proteins, including HCV RdRp. Here, we tested the effect of detergents on HCV RdRp activity in vitro and found that non-ionic (Triton X-100, NP-40, Tween 20, Tween 80, and Brij 35) and twitterionic (CHAPS) detergents activated HCV 1b RdRps by 8–16.6 folds, but did not affect 1a or 2a RdRps. The maximum effect of these detergents was observed at around their critical micelle concentrations. On the other hand, ionic detergents (SDS and DOC) completely inactivated polymerase activity at 0.01%. In the presence of Triton X-100, HCV 1b RdRp did not form oligomers, but recruited more template RNA and increased the speed of polymerization. Comparison of polymerase and RNA-binding activity between JFH1 RdRp and Triton X-100-activated 1b RdRp indicated that monomer RdRp showed high activity because JFH1 RdRp was a monomer in physiological conditions of transcription. Besides, 502H plays a key role on oligomerization of 1b RdRp, while 2a RdRps which have the amino acid S at position 502 are monomers. This oligomer formed by 502H was disrupted both by high salt and Triton X-100. On the contrary, HCV 1b RdRp completely lost fidelity in the presence of 0.02% Triton X-100, which suggests that caution should be exercised while using Triton X-100 in anti-HCV RdRp drug screening tests.

© 2012 Elsevier B.V. All rights reserved.

1. Introduction

Hepatitis C virus (HCV) belongs to the family *Flaviviridae* and has a positive-stranded RNA genome (Lemon et al., 2007). HCV chronically infects more than 130 million people worldwide (Wasley and Alter, 2000), and infection often induces liver cirrhosis and/or hepatocellular carcinoma (Kiyosawa et al., 1990; Saito et al., 1990). The 9.6-kb-long HCV RNA genome has a long open reading frame encoding a polyprotein of approximately 3,010 amino acids, which is processed into at least 10 viral proteins (NH_2-C-E1-E2-p7-NS2-NS3-NS4A-NS4B-NS5A-NS5B-COOH) by host and viral proteases (Grakoui et al., 1993; Hijikata et al., 1993). The 5′-untranslated region (UTR) contains the internal ribosome entry site (IRES) (Tsukiyama-Kohara et al., 1992). The 3′-UTR contains a poly pyrimidine "U/C" tract, a variable region, and 98-base X-region (Tanaka et al., 1996).

HCV RNA replication depends on the association between the viral protein and raft membranes (Shi et al., 2003; Aizaki et al., 2004), where NS5B RNA polymerase (RdRp) localizes by binding to sphingomyelin (Sakamoto et al., 2005). HCV RdRp is a key enzyme involved in the transcription and replication of the viral genome, and an important target of antivirals. Recently, we found that sphingomyelin bound to and activated HCV 1b RdRp, thereby recruiting the HCV replication complex into lipid raft structures (Weng et al., 2010).

Detergents are commonly used for solubilizing proteins from the lipid-containing components. Some restriction enzymes, reverse transcriptases, and Taq polymerases are stabilized by Triton X-100 or NP-40 (Weyant et al., 1990), while some other polymerases are activated by detergents (Thompson et al., 1972; Wu and Cetta, 1975; Hirschman et al., 1978). Triton X-100 is used for purification of HCV RdRp (Weng et al., 2009). Oligomerization of HCV RdRp is important for its activity (Qin et al., 2002; Clemente-Casares et al., 2011). We have developed an in vitro HCV de novo transcription system by using soluble RdRp and the complementary sequence of the 5′-HCV

Abbreviations: CHAPS, 3-[(3-cholanidopropyl)dimethylammonio]-1-propanesulfonate; CMC, critical micelle concentration; DOC, sodium deoxycholate; HCV, hepatitis C virus; IRES, internal ribosome entry site; KGlu, monopotassium glutamate; PMSF, phenylmethanesulfonyl fluoride; RdRp, RNA polymerase; SDS, sodium dodecyl sulfate; TNTase, terminal nucleotidyl transferase; UTR, untranslated region; nOG, octyl-β-glucoside.

* Corresponding author at: Choju Medical Institute, Fukushimura Hospital, 19-4 Azanakayama, Noyori-cho, Toyohashi, Aichi 441-8124, Japan. Tel.: +81 532 46 7511; fax: +81 532 46 8940.
E-mail address: toyoda_tetsuya@yahoo.co.jp (T. Toyoda).

0378-1119/$ – see front matter © 2012 Elsevier B.V. All rights reserved.
doi:10.1016/j.gene.2012.01.044

Author's personal copy

genome RNA (SL12-1S template) (Kashiwagi et al., 2002a; Kashiwagi et al., 2002b; Weng et al., 2009; Murayama et al., 2010; Weng et al., 2010). In this paper, we analyzed the effect of detergents on the activity and oligomerization of HCV RdRp, and found that non-ionic (Triton X-100, NP-40, Tween 20, Tween 80, and Brij 35) and twitterionic (3-[(3-cholanidopropyl)dimethylammonio]-1-propanesulfonate [CHAPS]) detergents activated HCV 1b RdRp. In addition, we analyzed the mechanism of RdRp activation by detergents and the relationship between RdRp oligomerization and its activity.

2. Materials and methods

2.1. Mutant HCV RdRp

The H502S mutation of HCR6 (1b) RdRp and the S502H mutation of JFH1 (2a) were introduced using an in vitro mutagenesis kit (Stratagene). Oligonucleotide sequence information is available upon request.

2.2. Purification of HCV RdRp from bacteria

HCV HCR6wt (1b) (Weng et al., 2009), NN (1b) (Watashi et al., 2005), Con1 (1b) (Binder et al., 2007), JFH1wt (2a) (Weng et al., 2009), J6CF (2a) (Murayama et al., 2007), H77 (1a) (Blight et al., 2003), RMT (1a), HCR6 (1b) H502S, and JFH1 (2a) H502S RdRps with a C-terminal 21-amino acid deletion were purified from bacteria as previously described with some modifications (Weng et al., 2009, 2010; Murayama et al., 2010). Briefly, HCV RdRps were eluted from Ni-NTA agarose (Qiagen) with 20 mM Tris–HCl (pH 8.0), 500 mM NaCl, 0.1% Triton X-100, 0.1% 2-mercaptoethanol, and 1 mM phenylmethanesulfonyl fluoride (PMSF) containing 250 mM imidazole after the column was washed with 5 mM imidazole. HCV RdRps were further purified through a Superdex 200 pg column (GE Healthcare) in 20 mM Tris–HCl (pH 8.0), 500 mM NaCl, 1 mM EDTA, 5 mM DTT, 10% glycerol, and 1 mM PMSF to remove contaminating nucleic acids (Fig. S1). The purified HCV RdRps were stored at −80 °C.

2.3. De novo HCV RdRp assay

HCV RdRp assay in the absence of primers was performed as described previously (Weng et al., 2009; Murayama et al., 2010). Briefly, following a 30-min pre-incubation period without ATP, CTP, or UTP, 100 nM HCV RdRp were incubated in 50 mM Tris–HCl (pH 8.0), 200 mM monopotassium glutamate (KGlu), 3.5 mM $MnCl_2$, 1 mM DTT, 0.5 mM GTP, 50 μM ATP, 50 μM CTP, 5 μM [α-^{32}P]UTP, 200 nM 184-nt model RNA template (SL12-1S) (Kashiwagi et al., 2002a; Weng et al., 2009; Murayama et al., 2010), 100 U/ml human placental RNase inhibitor, and the indicated amount of detergent at 29 °C for 90 min. [^{32}P]RNA products were separated in a 6% polyacrylamide gel containing 8 M urea. The resulting autoradiograph was analyzed with a Typhoon Trio Plus image analyzer (GE Healthcare) for the radio activity of 184-nt transcription products.

2.4. Kinetic analysis of HCV RdRp with and without Triton X-100

Kinetic analysis (measurement of *K*m and *V*max) was performed as previously published with and without 0.02% Triton X-100 (Kashiwagi et al., 2002b; Weng et al., 2009). For *K*m and *V*max of ATP, HCV RdRp was incubated in 50, 25, 10, 8, 5, 3, or 1 μM of ATP, 50 μM CTP, 0.5 mM GTP, 5 μM [α-^{32}P]UTP after preincubation in 0.5 mM GTP with and without 0.02% Triton X-100 at 29 °C for 60 min. For *K*m and *V*max of CTP, 50, 25, 10, 8, 5, 3, or 1 μM of CTP, 50 μM ATP, 0.5 mM GTP, and 5 μM [α-^{32}P]UTP, and for *K*m and *V*max of UTP, 50, 25, 10, 8, 5, 3, or 1 μM of UTP, 50 μM ATP, 0.5 mM GTP, 5 μM [α-^{32}P]CTP were used, respectively. For *K*m and *V*max of GTP, HCV RdRp was incubated in 500, 250, 100, 50, 25, 10, or 5 μM of GTP, 50 μM ATP, 50 μM CTP, 5 μM [α-^{32}P]UTP with and without 0.02% Triton X-100 without GTP preincubation.

2.5. Terminal nucleotidyl transferase (TNTase) assay

TNTase assay was performed with the heat denatured 5′-[^{32}P] sym/sub (5′-GAUCGGGCCCGAUC-3′) (Arnold and Cameron, 2000) with 0.5 mM GTP, 50 μM ATP, 50 μM CTP, and 50 μM UTP, and sym/sub with 0.5 mM GTP, 50 μM ATP, 50 μM CTP, and 5 μM [α-^{32}P]-UTP in the same experimental conditions as the above-described transcription assay (Hong et al., 2001). [^{32}P]RNA products were separated in a 15% polyacrylamide gel containing 8 M urea.

2.6. RNA filter-binding assay

RNA filter-binding assays were performed as previously described (Weng et al., 2009). Briefly, 100 nM of HCV RdRp and 100 nM [^{32}P] RNA template (SL12-1S) were incubated with the indicated amount of detergent in 25 μl of 50 mM Tris–HCl (pH 7.5), 200 mM KGlu, 3.5 mM $MnCl_2$, and 1 mM DTT at 29 °C for 30 min. After incubation, the solutions were diluted with 0.5 ml TE and filtered through nitrocellulose membranes (0.45 μm; Millipore). The filter was washed 5 times with TE, and the bound radioisotope was analyzed using the Typhoon Trio Plus image analyzer after being dried.

2.7. Western blot

Western blot analysis using a rabbit anti-HCV RdRp antibody was performed, as described previously (Kashiwagi et al., 2002b).

2.8. Gel filtration

The purified HCR6 (1b), J6CF (2a), and JFH1 (2a) RdRps (50 pmol) were applied on a Superdex 200 pg column in 50 mM Tris–HCl (pH 7.5), 200 mM KGlu or 150 mM NaCl, 3.5 mM $MnCl_2$, 1 mM DTT, and 0.2% glycerol with or without 0.1% Triton X-100.

2.9. Reagents

PMSF, Triton X-100, Tween 20, Tween 80, NP-40, Brij 35, octyl-β-glucoside (nOG), CHAPS, sodium deoxycholate (DOC), and sodium dodecyl sulfate (SDS) were obtained from Amresco; nucleotides were purchased from GE Healthcare; [α-^{32}P]UTP, [α-^{32}P]ATP, [α-^{32}P]GTP, [α-^{32}P]CTP, and [γ-^{32}P]ATP were from New England Nuclear.

2.10. Statistical analysis

Significant differences were determined using the Student's *t*-test.

3. Results

3.1. Effect of detergents on primer-independent HCV RdRp activity

First, we examined the effect of detergents on the primer-independent HCV RdRp activity in vitro (Fig. 1). HCR6 (1b) RdRpwt was activated by all the detergents tests, except octyl-β-glucoside (nOG), but JFH1 (2a) RdRpwt was not. The activation curves of HCR6 (1b) RdRpwt by these detergents plateaued at certain concentrations: 0.002 or 0.004% Triton X-100, 0.001% NP-40, 0.005% Tween 20, 0.001% Tween 80, 0.001% Brij 35, and 0.1% CHAPS. HCR6 (1b) RdRp activity decreased at concentrations greater than 1% Triton X-100, and 30% Triton X-100 completely inhibited HCR6 (1b) RdRpwt activity (Fig. 1A, right panel). With an activation ratio of about 2 at 0.1%, nOG weakly activated HCR6 (1b) RdRpwt. At 0.5% nOG, the

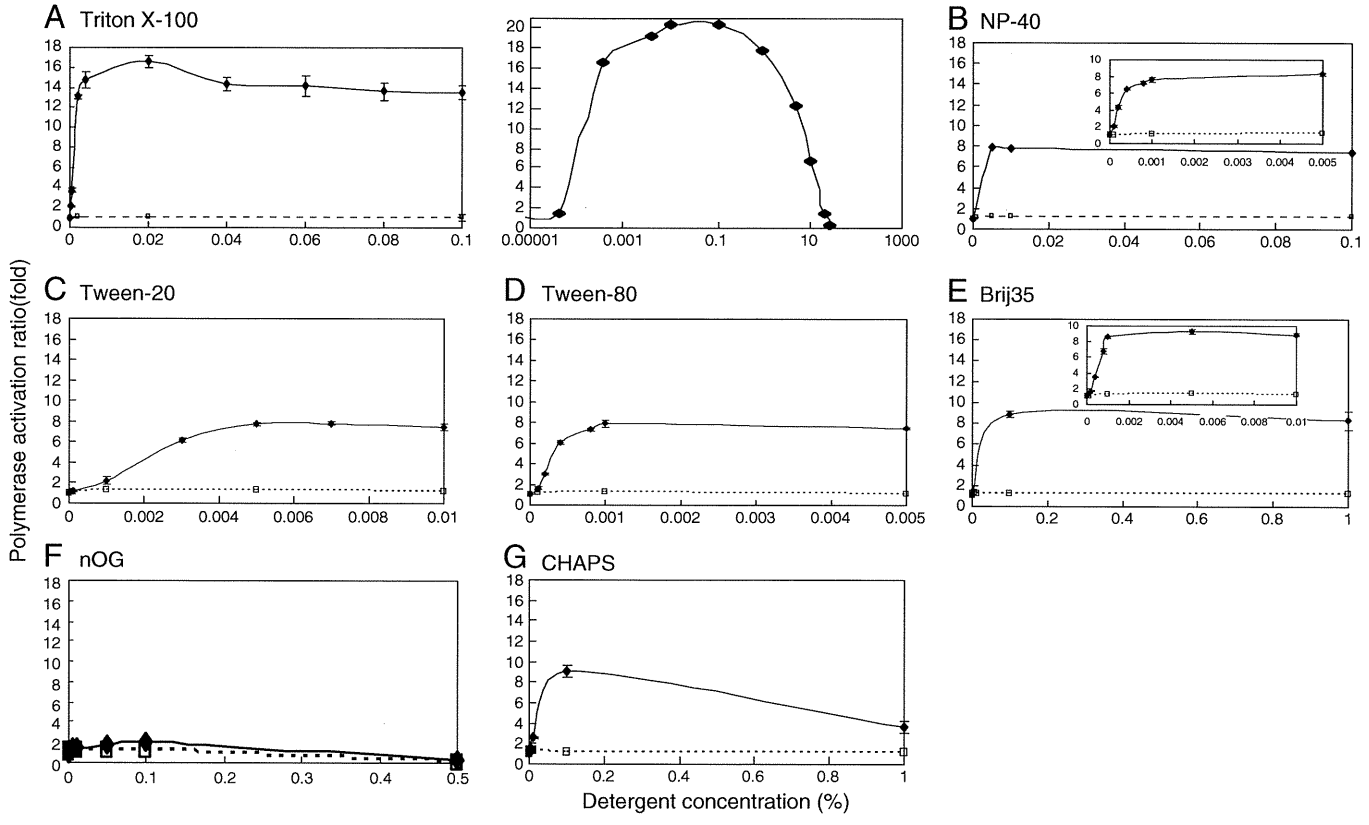

Fig. 1. The effect of detergents on HCV HCR6 and JFH1 RNA polymerases. Wild-type HCR6 (1b) and JFH1 (2a) RdRps were assayed with 0.000004, 0.00004, 0.0004, 0.004, 0.01, 0.02, 0.04, 0.06, 0.08, and 0.1% Triton X-100 (A, left panel); 0.0001, 0.0002, 0.0004, 0.0008, 0.001, 0.005, 0.1, and 0.5% NP-40 (B); 0.0001, 0.001, 0.003, 0.005, 0.007, and 0.01% Tween 20 (C); 0.0001, 0.0002, 0.0004, 0.0008, 0.001, and 0.005% Tween 80 (D); 0.0001, 0.0002, 0.0004, 0.0008, 0.001, 0.005, 0.01, 0.1, and 1% Brij 35 (E); 0.001, 0.005, 0.01, 0.05, and 0.1% nOG (F); or 0.0001, 0.001, 0.005, 0.01, 0.1, 0.1, and 1% CHAPS (G). The effect of high concentration of Triton X-100 on HCR6 (1b) RdRpwt is shown in A (right panel). Inset: Polymerase activation ratio at a lower concentration of NP-40 (B), and Brij 35 (E). Mean and standard deviation (error bar) of the polymerase activation ratio were calculated from 3 independent experiments. The solid line indicates the activation ratio of HCR6 (1b) RdRpwt, and the broken line indicates that of JFH1 (2a) RdRpwt.

activation ratio of HCR6 (1b) RdRpwt was 0.3. At 1% of CHAPS, the activity of HCR6 (1b) RdRpwt was increased by 3.6 folds. The detergent concentration that most activated HCR6 (1b) RdRpwt was approximate to the critical micelle concentration (CMC; Table 1).

When the activation ratios of detergents on HCR6 (1b) RdRpwt were compared, that of Triton X-100 was the highest (Fig. 2, Table 1). Other non-ionic detergents and CHAPS activated HCR6 (1b) RdRpwt to an extent equal to about half of Triton X-100 activation. Although a non-ionic detergent, nOG barely activated HCR6 (1b) RdRpwt.

Because 0.02% Triton X-100 maximally activated HCR6 (1b) RdRpwt, we compared its activation effect on other HCV RdRps (Fig. 3, Table 2). JFH1 (2a) RdRpwt showed the strongest RdRp activity, which is in accordance with previous reports (Weng et al., 2009; Murayama et al., 2010; Schmitt et al., 2011). The RdRp activities of 1b HCR6 and NN activated by Triton X-100 were similar to that of JFH1 RdRpwt in the absence of detergents (Fig. 3B), whereas the RdRp activity of Triton X-100-activated 1b Con1 was about half of that of wild-type JFH1. Neither 1a nor 2a RdRps were activated by Triton X-100.

Table 1
CMC and HCV HCR6 (1b) RdRpwt activation ratio of different detergents.

Detergent	CMC[a] in H_2O (%)	Minimal concentration of maximal activation (%)	Maximal activation (folds)[b]
Triton X-100	0.0155	0.02	16.6 ± 0.56
NP-40	0.0179	0.005	8.3 ± 0.18
Tween 20	0.0074	0.007	7.8 ± 0.21
Tween 80	0.0016	0.001	8.0 ± 0.22
Brij 35	0.1103	0.1	9.2 ± 0.34
nOG	0.672–0.730	0.1	2.1 ± 0.35
CHAPS	0.492–0.615	0.1	9.1 ± 0.60

[a] Modified from "TECHNICAL RESOURCE" (Pierce).
[b] Calculated from Fig. 2.

3.2. RNA template binding with Triton X-100

Next, we compared the template RNA-binding activity of 1a, 1b, and 2a RdRps in the presence of Triton X-100 by using the [^{32}P] SL12-1S model RNA template (Kashiwagi et al., 2002a; Weng et al., 2009, 2010; Murayama et al., 2010) in order to examine the transcription steps activated by Triton X-100 (Fig. 4, Table 2). Template RNA binding was the first step of transcription. The RNA-binding activity of JFH1 RdRpwt was the highest without Triton X-100 (data not shown) (Weng et al., 2009). Different from RdRp activity, the RNA-binding activity of all HCV RdRps was somehow activated by 0.02% Triton X-100. The RNA-binding activity of 1b RdRps was increased by 7–10 folds with Triton X-100.

3.3. Gel filtration of 1b and 2a RdRps

Proteins are generally soluble in detergents. Because HCR6 (1b) RdRpwt showed similar polymerase activity with Triton X-100 as JFH1 (2a) RdRpwt without Triton X-100, we compared the oligomerization state of these RdRps. The oligomerization state of HCR6 (1b) and JFH1 (2a) RdRps under transcription (physiological) conditions (200 mM KGlu or 150 mM NaCl) was analyzed by gel filtration on

Author's personal copy

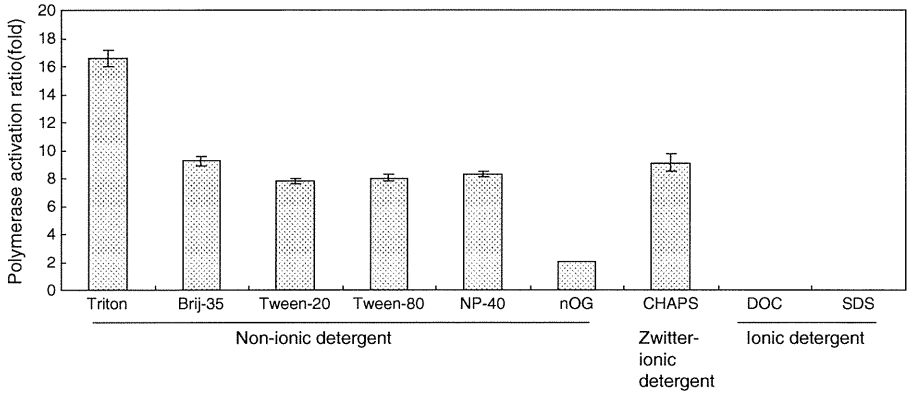

Fig. 2. Activation effect of HCV HCR6 polymerase with detergents at CMC. HCV HCR6 (1b) RdRpwt was assayed at CMC in the presence of Triton X-100 (0.02%), Brij 35 (0.1%), Tween 20 (0.007%), Tween 80 (0.001%), NP40 (0.005%), nOG (0.1%), CHAPS (0.1%), DOC (0.001%), and SDS (0.001%). The activation ratio (fold) is indicated in Table 2. Mean and standard deviation (error bar) of the polymerase activity relative to that without detergent were calculated from 3 independent experiments.

Superdex 200 (Figs. 5 and 6). HCR6 (1b) RdRpwt was eluted from the void volume fraction to the 158-kDa fraction without Triton X-100 (Fig. 5A), which meant that HCR6 (1b) RdRpwt formed random oligomers. It was eluted in the 38-kDa fraction with 0.1% Triton X-100 (Fig. 5B), which indicated that it was smaller than its monomer gel filtration size (Fig. S1D). However, JFH1 (2a) RdRpwt was eluted in the slightly larger fraction (80 kDa) than other HCV RdRps with or without Triton X-100, which indicated the monomer size (Figs. 5C and D, S1F). From the gel filtration and transcription data of HCR6 (1b) RdRpwt and JFH1 (2a) RdRpwt, it was concluded that Triton X-100 dispersed HCR6 (1b) RdRpwt, and that the higher-ordered oligomers of HCR6 (1b) RdRpwt were inactive. Triton X-100 might also affect the interaction between HCR6 (1b) RdRpwt and Superdex200 gel matrix because it was eluted in the smaller molecular weight fractions with Triton X-100 than the monomer gel-filtration size in 0.5 M NaCl (76 kDa, Fig. S1D). Western blot analysis indicated that these RdRp were not degraded (Figs. 5A and B, inset).

Qin et al. found that amino acids 18E and 502H interacted with each other to form the HCV 1b RdRp oligomer/dimer (Qin et al., 2002). Only 2a RdRps harbor the amino acid S at position 502, contrary to other genotype forms of RdRps, which harbor the amino acid H at that same position (Table S1). Therefore, we first examined

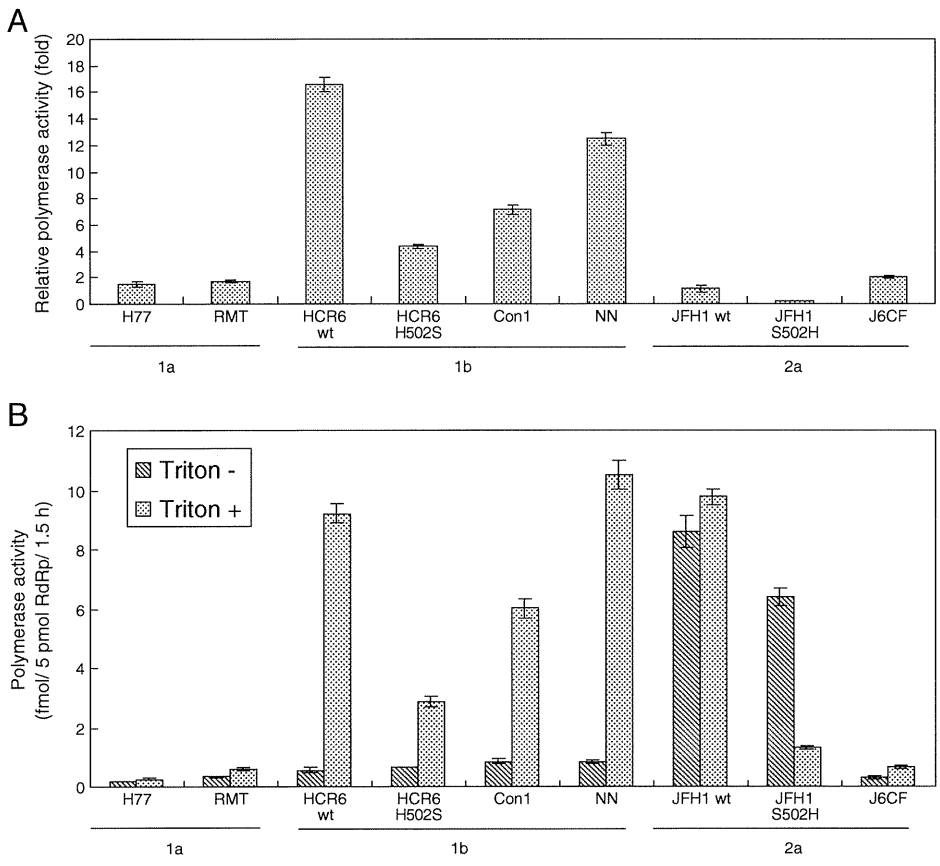

Fig. 3. Effect of 0.02% Triton X-100 on various HCV RNA polymerases. HCV H77 (1a), RMT (1a), HCR6 (1b) wt and H502S, NN (1b), Con1 (1b), JFH1 (2a) wt and S502H, and J6CF (2a) RdRps were assayed in the presence or absence of Triton X-100. A: Activation ratio (fold) of RNA polymerase activity. B: Polymerase activity (fmol of NMP/5 pmol RdRp/1.5 h) in the presence or absence of Triton X-100. Mean and standard deviation (error bar) of the polymerase activity were calculated from 3 independent experiments.

Author's personal copy

Table 2
Relative activation ratio of HCV RdRp by Triton X-100.

Genotype	1a		1b			2a	
Name	H77	RMT	HCR6	Con1	NN	JFH1	J6CF
Polymerase activity (folds)[a]	1.5 ± 0.17	1.7 ± 0.11	16.6 ± 0.56	7.1 ± 0.38	12.5 ± 0.48	1.1 ± 0.28	2.0 ± 0.12
RNA template-binding activity (folds)[b]	3.8 ± 0.11	3.9 ± 0.18	9.6 ± 0.39	7.9 ± 0.41	6.9 ± 0.16	2.2 ± 0.14	3.4 ± 0.21

[a] Activation ratio of polymerase activity was calculated on the basis of the data represented in Fig. 3A.
[b] Activation ratio of RNA template-binding activity was calculated on the basis of the data represented in Fig. 4A.

another 2a RdRp, J6CF (2a) RdRp, by gel filtration (Fig. 5E). J6CF (2a) RdRp was also eluted as a monomer in 150 mM NaCl buffer without Triton X-100. These gel filtration data was in agreement with the intermolecular interaction and random oligomerization of HCV RdRp caused by 18E and 502E (Qin et al., 2002). Amino acid 18E is shared by HCV RdRps of all 6 genotypes (Table S1) (Clemente-Casares et al., 2011). Therefore, in order to confirm the importance of 502H for oligomerization of HCV RdRp, S502H and H502S mutations were introduced into JFH1 (2a) and HCR6 (1b) RdRps, respectively, and analyzed by gel filtration (Fig. 6). JFH1 (2a) RdRpS502H formed oligomers, and HCR6 (1b) RdRpH502S was eluted in the 15-kDa fraction, which was smaller than its monomeric gel-filtration size. JFH1 (2a) RdRpS502H was eluted around the 50-kDa position with Triton X-100. The RdRp dimers (Qin et al., 2002) were not found in any of our gel filtration profiles. Western blot analysis indicated that the proteins were not degraded (Fig. 6, inset).

The effect of these mutations in RdRp and RNA template-binding activity with and without Triton X-100 was examined (Figs. 3 and 4). JFH1 (2a) RdRpS502H RdRp activity was lower than that of the wild-type in the absence of Triton X-100. Different from the Triton X-100 activation effect on HCR6 (1b) RdRpwt, JFH1 (2a) RdRpS502H RdRp activity decreased, while its RNA template binding increased, in the presence of Triton X-100. HCR6 (1b) RdRpH502S RdRp activity was similar to that of the wild-type, but less activated by Triton X-100 than by the wild-type. RNA template-binding activity of HCR6 (1b) RdRpH502S was activated 2.3 times by Triton X-100.

The 502 mutation data indicated that 502H is important for oligomerization of 1b RdRp molecules in the transcription (physiological salt) condition. Triton X-100 prevented the oligomerization of 1b RdRps by 502H. Moreover, For HCR6 (1b) RdRpwt, the 38-kDa gel filtration molecules (Fig. 5B), which might correspond to the monomer, were more active than the oligomer molecules.

3.4. Fidelity of HCV RdRp with Triton X-100

Finally, we aimed to calculate the kinetic constants (*K*m and *V*max) of HCR6 (1b) RdRp in the presence of 0.02% Triton X-100 because the activation ratio of the polymerase activity was higher than that of RNA binding of HCR6 (1b) RdRp. When nucleotide concentration was low, the amount of product without Triton X-100 decreased; this data can be used to draw Lineweaver–Burk plot (Weng et al., 2009). However, with Triton X-100, the product amount did not decrease according to the decrease of each nucleotide (Fig. 7A). Moreover, each of the nucleotide substrates was removed from the standard HCV in vitro transcription condition (Fig. 7B). Although ATP, CTP or UTP were removed from the reaction buffer, HCV HCR6 (1b) RdRp transcribed the same 184-nt products with Triton X-100, which disappeared without Triton X-100. When GTP was removed, no products were observed with or without Triton X-100 because HCV RdRp required GTP for its structure (Bressanelli et al., 2002). These kinetic experiments indicated that HCV HCR6 (1b) RdRp completely lost fidelity with Triton X-100.

Terminal nucleotidyl transferase (TNTase) activity has been sometimes detected in HCV 1b RdRp preparations (Behrens et al., 1996; Ranjith-Kumar et al., 2001; Ranjith-Kumar et al., 2004; Vo et al., 2004). TNTase activity was not detected in our system, in which the model RNA template contains a CCC-3′ at the 3′-end (Kashiwagi et al., 2002b; Weng et al., 2009). Nevertheless, we examined whether TNTase activity was detected with Triton X-100 using sym/sub, which has GpG-primed transcription activity, but we failed to observe any de novo initiation activity (Hong et al., 2001). No mobility shift was shown by 5′-[^{32}P]sym/sub or sym/sub incubated with [^{32}P]UTP on polyacrylamide gel electrophoresis (PAGE) (Figs. 7C and D), indicating that no TNTase activity was detected in our system with or without Triton X-100.

Apparent *K*m and *V*max of HCR6 (1b) RdRp with Triton X-100 for GTP was 303 ± 15.1 μM and 6.21 ± 0.225/min, respectively (Fig. S3).

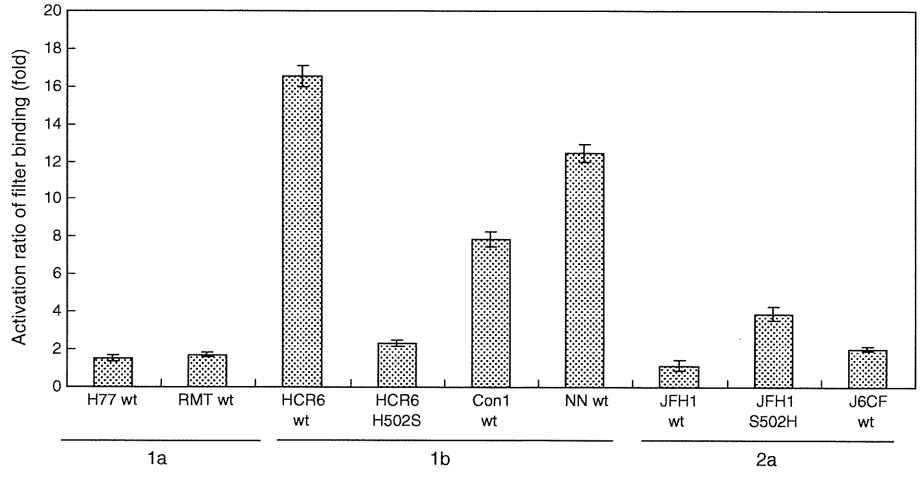

Fig. 4. Effect of 0.02% Triton X-100 on the RNA template-binding activity of HCV RNA polymerases. One hundred nanomolars each of HCV H77 (1a), RMT (1a), HCR6 (1b), NN (1b), Con1 (1b), JFH1 (2a), and J6CF (2a) RdRps with [^{32}P]RNA templates (SL12-1S) were filtered through nitrocellulose membranes after incubation with or without Triton X-100. Mean and standard deviation (error bar) of the RNA filter binding activation (folds) were calculated from 3 independent experiments.